Quantum Inf Process
DOI 10.1007/s11128-015-1161-3

Sympathetic cooling in a large ion crystal

Guin-Dar Lin[1] · **L.-M. Duan**[2,3]

Received: 19 October 2014 / Accepted: 17 October 2015

Abstract We analyze the dynamics and steady state of a linear ion array when some of the ions are continuously laser cooled. We calculate the ions' local temperature measured by its position fluctuation under various trapping and cooling configurations, taking into account background heating due to the noisy environment. For a large system, we demonstrate that by arranging the cooling ions evenly in the array, one can suppress the overall heating considerably. We also investigate the effect of different cooling rates and find that the optimal cooling efficiency is achieved by an intermediate cooling rate. We discuss the relaxation time for the ions to approach the steady state, and show that with periodic arrangement of the cooling ions, the cooling efficiency does not scale down with the system size.

Keywords Sympathetic laser cooling · Paul trap · Quantum gate error · Large-scale quantum computing

1 Introduction

Trapped ions constitute one of the leading systems for implementation of quantum computation. Numerous advances have been achieved in this system, including realization of faithful quantum gates [1–7], preparation of many-body quantum states [8–15], and quantum teleportation [16,17]. There are also developments to scale up this system, based on either ion shuttling [18–20] or quantum networks [21–26]).

✉ Guin-Dar Lin
guindarl@phys.ntu.edu.tw

1 Center for Quantum Science and Engineering, and Department of Physics, National Taiwan University, Taipei 10617, Taiwan

2 Department of Physics, University of Michigan, Ann Arbor, MI 48109, USA

3 Center for Quantum Information, IIIS, Tsinghua University, Beijing 100084, China

Published online: 03 November 2015

In a typical ion trap, the ions are first Doppler cooled and form a crystal. Most of the quantum computation experiments use a one-dimensional ion crystal. The ions may be subjected to further sub-Doppler cooling, such as sideband cooling. However, the difficulty of sideband cooling scales up with the number of phonon modes, which increase with the number of ions [27–29]. It has been shown that in principle high-fidelity quantum computation can be achieved even at the Doppler temperature by employing the ions' transverse phonon modes [29,30]. In a real experimental setup, the ions are subject to substantial background heating. For long-time quantum computation, to have the ions constantly remain at a certain temperature, it requires sympathetic cooling [31,32], in which case a subset of ions (cooling ions) are continuously laser cooled, bringing down the temperature of other ions (the computational ions) through the heat propagation enabled by the Coulomb interaction in the ion crystal. Sympathetic cooling has been studied for small systems with a few ions [33–35].

In this paper, we study the effectiveness of sympathetic cooling in a large one-dimensional ion crystal. Although in general temperature is not well defined for this system as it does not reach a thermal equilibrium state, as a relevant indicator for quantum computation, we measure the local "temperature" of the ions through their average position fluctuation (PF) $\delta x_i^{\xi} \equiv \sqrt{\langle x_i^{\xi 2}\rangle}$ (for the ith ion) with $\xi = x, y$ for the transverse phonon modes and $\xi = z$ for the axial modes. This position thermal fluctuation is an important indicator for fidelity of quantum gates. We discuss two different arrangements of the cooling ions: edge cooling and periodic-node cooling. In the former case, the ions at the two edges of an ion array are continuously laser cooled. In the latter case, the cooling ions are distributed evenly and periodically in the ion chain. We show that the periodic-node cooling is much more effective than the edge cooling. For a large crystal, the edge cooling becomes very inefficient. We then discuss the non-trivial dependence of the local temperature of the computational ions on the cooling rate of the cooling ions. A large cooling rate does not necessarily lead to more efficient cooling of the computational ions. Instead, there is an intermediate optical cooling rate, in agreement with our previous observation [36]. We finally investigate the timescale for the system to reach the steady state, which in general differs from the thermal equilibrium state [36].

This paper is organized as follows. In Sect. 2, we present the Heisenberg-Langevin equations to describe the driven dynamics of a many-ion array and provide their formal exact solutions. In Sect. 3, we discuss the motional steady states of the ions under background heating and continuous sympathetic cooling on the cooling ions. In Sect. 4, we study different cooling configurations and discuss the corresponding cooling efficiency. In Sect. 5, we investigate how the cooling performance of the sympathetic cooling depends on the laser cooling rate. In Sect. 6, we study the relaxation dynamics of the cooling process and discuss the timescale of relaxation as well as its scaling with the system size. Finally, we summarize the major findings in Sect. 7.

2 Formalism

Consider an ion string confined in an RF trap with an effective static potential $\mathcal{V}(\mathbf{r}) = \frac{1}{2}m\omega_x^2(x^2 + y^2) + V(z)$. For a small crystal, the axial confinement is usually

approximated by $V(z) = \frac{1}{2}m\omega_z^2 z^2$ with $\omega_z \ll \omega_x$ so that the one-dimensional alignment is stabilized. For a large crystal, the axial potential might take an anharmonic form [29]. Trapped ions have collective motion around their classical equilibrium positions. Assuming that each ion is coupled to its respective thermal bath (corresponding to either cooling or background heating), we describe the driven ion array by the following Heisenberg-Langevin equations:

$$\begin{cases} \dot{x}_i^{\xi} = p_i^{\xi} \\ \dot{p}_i^{\xi} = -\sum_j A_{ij}^{\xi} x_j^{\xi} - \gamma_i^{\xi} p_i^{\xi} + \sqrt{2\gamma_i^{\xi}}\,\zeta_i^{\xi}(t) \end{cases}, \tag{1}$$

where $i, j = 1, ..., N$ are ion indices, $\xi = x, y, z$ stands for the mode directions, and $A_{ii}^{\xi} = \beta_i^{\xi} - \sum_{j(\neq i)} \frac{C_{\xi}}{\left|z_j^0 - z_i^0\right|^3}$, $A_{ij}^{\xi} = \frac{C_{\xi}}{\left|z_j^0 - z_i^0\right|^3} (i \neq j)$ with $\beta_i^{x,y} = \omega_x^2$, $\beta_i^z = \partial^2 V/\partial z_i^2$, $C_{x,y} = 1$, $C_z = -2$, and z_i^0 denotes the ith ion's axial equilibrium position. We take the ion spacing d_0 as the length unit[1], e^2/d_0 as the energy unit, and $\omega_0 \equiv \sqrt{e^2/(md_0^3)}$ as the frequency unit so that the quantities in Eq. (1) are dimensionless. For the convenience of discussion, we drop the superscript ξ. Since the transverse and axial modes are decoupled, the derivation simply applies to any direction. A random kick $\zeta_i(t)$ associated with the driving rate γ_i can be expressed as $\zeta_i = -i\sum_k \sqrt{\frac{\omega_k}{2}} G_{ik}(b_k - b_k^{\dagger})$ (in units of $\sqrt{\hbar m\omega_0}$), where G is the canonical transformation matrix which diagonalizes A, i.e., $G^{\top} A G = A^D$ is diagonalized, and b_k is the bosonic field operator of the kth motional mode with frequency ω_k. For a Markovian bath, $b_k(t)$ satisfies $\left\langle b_k^{\dagger}(t_1) b_{k'}(t_2)\right\rangle = n_k^B(T)\delta_{kk'}\delta(t_1 - t_2)$ with $n_k^B(T) \equiv \left[\exp(\omega_k/T) - 1\right]^{-1}$ the phonon number of the kth mode for a given temperature T (in units of $\hbar\omega_0/k_B$). It is then straightforward to show that the correlation of the driving force is given by $\left\langle \zeta_i(t)\zeta_j(t')\right\rangle = \delta_{ij}\delta(t - t')\sum_k \omega_k G_{ik}^2 \left(n_k^B(T) + \frac{1}{2}\right)$. In our current case, where each ion couples to an independent reservoir T_i, it is reasonable to assume that the ion i feels a local bath with $\left\langle \zeta_i(t)\zeta_j(t')\right\rangle = \delta_{ij}\delta(t - t')\Theta_i(T_i)$ and $\Theta_i(T_i) \equiv \sum_k \omega_k G_{ik}^2 \left(n_k^B(T_i) + \frac{1}{2}\right)$. The solution to Eq. (1) is given by $\mathbf{q}(t) = e^{-\Omega t}\mathbf{q}(0) + \int_0^t d\tau e^{\Omega(\tau - t)}\eta(\tau)$, where $\mathbf{q} \equiv (x_1, x_2, ...; p_1, p_2, ...)^{\top} = \begin{bmatrix} \{x_i\} \\ \{p_i\} \end{bmatrix}$, $\eta(t) \equiv \begin{bmatrix} \{0\} \\ \left\{\sqrt{2\gamma_i}\zeta_i\right\} \end{bmatrix}$, and $\Omega \equiv \begin{bmatrix} 0 & -I \\ [A_{ij}] & [\gamma_i\delta_{ij}] \end{bmatrix}$ is a $2N \times 2N$ matrix which can be diagonalized as $\left[U^{-1}\Omega U\right]_{\alpha\beta} = \lambda_{\alpha}\delta_{\alpha\beta}$. We then obtain the variation of operators x_i and p_i:

[1] Here, the choice of d_0 is somewhat arbitrary as long as it characterizes the length scale of the inter-ion spacing. In this article, we define d_0 differently in various situations. For instance, in a small harmonic trap ($N = 20$), we choose d_0 to be the smallest spacing in the middle of the chain. In a large non-uniform ion crystal ($N = 121$), we choose $d_0 = \frac{1}{100}\sum_{i=11}^{110}(z_{i+1}^0 - z_i^0)/100$, a mean value of all ion spacings except that 10 large ones on the edges are excluded.

$$\langle q_\mu^2\rangle = \sum_{s=1}^{N}\sum_{\alpha,\beta=1}^{2N} U_{\mu\alpha}U_{\mu\beta}\Big(e^{-(\lambda_\alpha+\lambda_\beta)t}\Big[\langle x_s^2(0)\rangle U_{\beta s}^{-1}U_{\alpha s}^{-1} + \langle p_s^2(0)\rangle U_{\beta,s+N}^{-1}U_{\alpha,s+N}^{-1}\Big] + \Big(1-e^{-(\lambda_\alpha+\lambda_\beta)t}\Big)\frac{2\gamma_s\Theta_s}{\lambda_\alpha+\lambda_\beta}U_{\beta,s+N}^{-1}U_{\alpha,s+N}^{-1}\Big), \tag{2}$$

where $\mu = 1, 2, ..., N$ correspond to x-operators, $\mu = N+1, N+2, ..., 2N$ correspond to p-operators.

For trapped ion quantum computing, the computational fidelity is determined by the ion PF $\delta x_i^{\xi} \equiv \sqrt{\langle x_i^{\xi 2}\rangle}$ (denoted by δx_i and δz_i for transverse and axial motion, respectively). When the quantum gate is operated by means of the transverse modes, the estimated infidelity is $\delta F_i^x \sim \pi^2\eta_i^4/4$ [3,29,30], where the Lamb Dicke parameter $\eta_i \sim |\Delta\mathbf{k}|\,\delta x_i$ with $\Delta\mathbf{k} \parallel \hat{x}$ the wavevector difference in the two Raman beams. Another possible source of error comes from the spatial non-uniformity of the laser intensity when a single beam addresses a specific ion; the ion's axial motion results in variation in the actual Rabi frequency. This error is estimated by $\delta F_i^z \sim \pi^2(\delta z_i/w)^4/2$ given that the laser beam's Rabi frequency is approximated by a Gaussian profile $\Omega(z) \propto e^{-((z-z_i^0)/w)^2}$ with width w [29]. Both of the gate errors are determined by the position thermal fluctuation δx_i or δz_i of the ions. So, in the following discussion, we focus on the distribution of the ion position fluctuation δx_i or δz_i in the array.

3 Steady-state distribution

3.1 Thermal equilibrium

We first look at the thermal equilibrium distribution of the ion chain when the whole system is driven by a thermal field with a well-defined temperature. From $x_i = \alpha\sum_k G_{ik}\sqrt{\frac{1}{2\omega_k}}(a_k^\dagger + a_k)$ where $\alpha \equiv \sqrt{\hbar/(m\omega_0)}/d_0$ is the length conversion factor and a_k ($a_k^\dagger$) is the annihilation (creation) operator of mode k, we obtain $\langle x_i^2\rangle = \alpha^2\sum_k \frac{G_{ik}^2}{\omega_k}\left(n_k^B(T)+\frac{1}{2}\right) = \alpha^2\sum_k \frac{G_{ik}^2}{2\omega_k}\coth\left(\frac{\omega_k}{2T}\right)$. In Fig. 1, we show the distribution of δx_i and δz_i in a harmonic trap for both the axial and transverse motions at the Doppler temperature T_D, and their contribution to the corresponding gate infidelities [29]. In this case, the axial fluctuation δz_i varies in space, suggesting that the longitudinal motion of the whole ion chain is "more collective" and relies on the global geometry. Supposing that a single ion is subjected to a different temperature, its longitudinal movement does not directly reveal information of the temperature associated with the local bath because neighboring ions subjected to their own baths may interfere through collective modes. On the contrary, its transverse movement directly reflects the local temperature. This is because the axial and transverse modes are decoupled, and for each ion, the energy scale set by the transverse confinement $\hbar\omega_x$ is dominant over other scales. Note that the diagonal terms of A^x are more significant than the off-diagonal

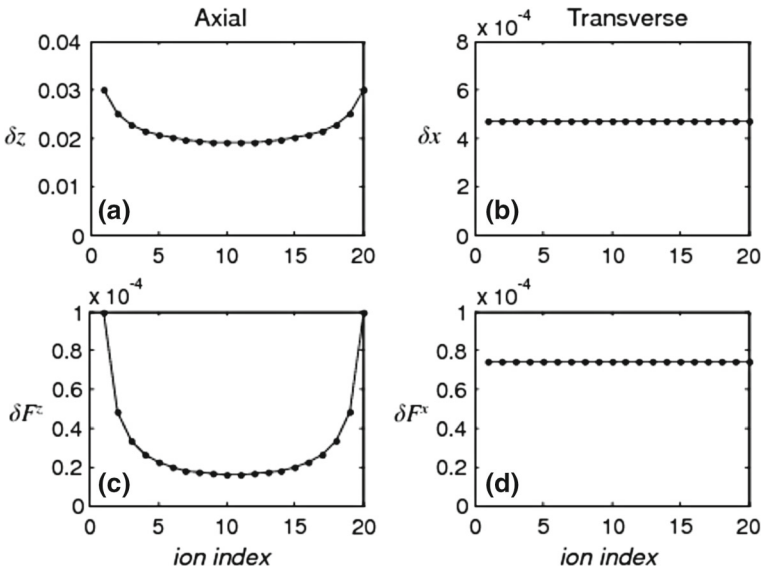

Fig. 1 **a**, **b** Thermal equilibrium distributions of the averaged ion PF in units of d_0 and **c**, **d** the associated computational infidelity corresponding to the axial and transverse motion at the Doppler temperature $k_B T_D/\hbar = 2\pi \times 9.9\,\text{MHz}$ for 20 $^{171}\text{Yb}^+$ ions. Other parameters: $\omega_x = 2\pi \times 5.1\,\text{MHz}$, $\omega_z = 2\pi \times 34\,\text{kHz}$, $|\Delta\mathbf{k}|d_0 = 157$ with $d_0 = 10\,\mu\text{m}$, the minimal ion spacing in the middle of the chain

ones, meaning that the "local modes" defined by x_i and p_i^x can be discussed separately from those at different sites, with only small corrections due to inter-ion coupling. This is where the concept of a "local temperature" for a single ion starts to make sense. Such consideration has also motivated our investigation about the validity of classical thermal transportation for the trapped ion system [36]. Each ion can then be approximated as an harmonic oscillator weakly coupled to others, whose "local" phonon occupation number is given by $n_i = \frac{\alpha^{-2}}{2}(\omega_x \langle x_i^2\rangle + \omega_x^{-1}\langle p_i^{x2}\rangle - 1) \approx \alpha^{-2}\omega_x \langle x_i^2\rangle - \frac{1}{2}$. In the case shown in Fig. 1, PF$= 10^{-3}d_0$ corresponds to $n_i = 8.5$ with $\alpha = 2.0 \times 10^{-3}$.[2]

3.2 Steady-state profile under sympathetic cooling

If different parts of the system make contact with reservoirs at different temperatures, as relevant for sympathetic cooling, the local temperature of the ions in the steady state will in general have a non-uniform spatial profile. In this section, we investigate this steady-state profile.

We first examine an example where the two edge portions of the ion chain are continuously laser cooled (we assume Doppler cooling, although the formalism also applies to other kinds of sympathetic cooling). The rest of the ion chain is driven by a hot bath corresponding to the background heating. According to Eq. (2), in the

[2] Throughout this article, we choose ytterbium 171 ions spaced by $d_0 = 10\,\mu\text{m}$ as examples, so $\omega_0 = 9.0\,\text{MHz}$ and $\alpha = 2.0 \times 10^{-3}$.

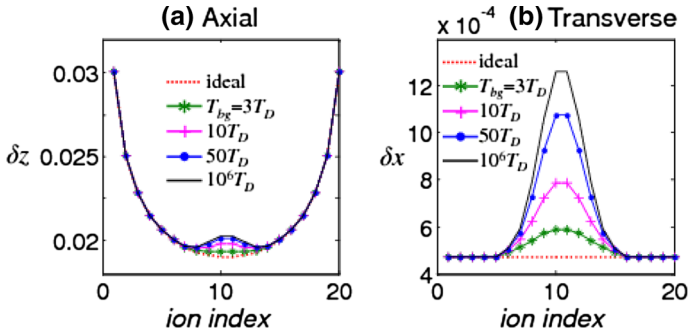

Fig. 2 (Color online) Steady-state distributions of the ion PF in a harmonic trap under different background temperature for a given constant heating rate. As a comparison, the ideal (no background heating, $\gamma_{bg} = 0$) curves are shown in *red dotted lines*

long-time limit, a steady state should be reached, providing a time-invariant profile of the position fluctuation δx_i or δz_i over all the ions.

To model the effect of background heating, we assume a small value for the background driving rate γ_{bg} with respect to the associated environment temperature T_{bg}. The value of T_{bg} is hard to quantify; the actual experimentally accessible parameter is the creation rate of phonons for a given motional mode k, that is, $\gamma_{bg} n_k^B \sim \gamma_{bg} T_{bg}/\omega_k$. To simplify our discussion, we treat the generated phonon numbers approximately the same around the range of all transverse (axial) modes. In other words, the background heating is now only characterized by $\kappa \equiv \gamma_{bg} T_{bg}$. Nevertheless, for a given value of κ, we still have the freedom to vary T_{bg} (and hence γ_{bg}) while keeping κ a constant parameter. As an example, we here consider an $N = 20$ chain with 5 ions on both ends as cooling ancillas. By denoting the set of the cooling ancillary ions by C and rest of the chain by H, we take $T_i = T_{bg}$, $\gamma_i = \kappa/T_{bg}$ for $i \in H$ and $T_i = T_D$, $\gamma_i = 0.1$ for $i \in C$. We then compare the resultant steady-state profile of δx_i and δz_i under various T_{bg} in Fig. 2 with constant $\kappa = 10^{-4}$, which amounts to a heating rate of about 60 phonons per second per ion for the lowest axial mode of $2\pi \times 34$ kHz. Note that in a real ion trap, a typical heating rate is about 100–1000 photons per second. As expected, the PF of the ancillary ions coincides with their supposed thermal equilibrium values at the Doppler temperature T_D while δx_i and δz_i show a hump in the middle part of the distribution due to the background heating. For T_{bg} set to larger values, the hump grows but asymptotically converges to a fixed profile, providing an *upper bound* of the profile. This corresponds to the "worst" case with the largest contribution to the gate infidelity. In the following, we only show such upper bounds for all the circumstances and investigate the discrepancy between these bounds and the fluctuation profile at the Doppler temperature (corresponding to the perfectly cooled case).

4 Comparison of different cooling configurations

In this section, we compare the efficiency of sympathetic cooling under two cooling configurations: edge cooling and periodic-node cooling. For each case, we show the

results under both harmonic and anharmonic axial traps. For a large ion crystal, the inhomogeneous ion spacing under a harmonic trap complicates the gate design and reduces its fidelity for quantum computation. To overcome this problem, as suggested in [29], it is better to use anharmonic traps which can give equal or almost equal spacing for the ions in the chain. We consider two kinds of anharmonic trap: the one (called the uniform trap for simplicity of terminology) which gives perfect uniform spacing for the ions and the quartic trap with potential $V(z) = \frac{1}{2}\alpha_2 z^2 + \frac{1}{4}\alpha_4 z^4$ which gives approximate uniform ion spacings. The parameters α_2 and α_4 in $V(z)$ are chosen to minimize the variation in the distribution of the ion spacings in the chain [29].

4.1 Edge cooling

First, we show the result with the edge segments of the ions are Doppler cooled. Figure 3 shows the final distributions of δx_i and δz_i under three different traps. As

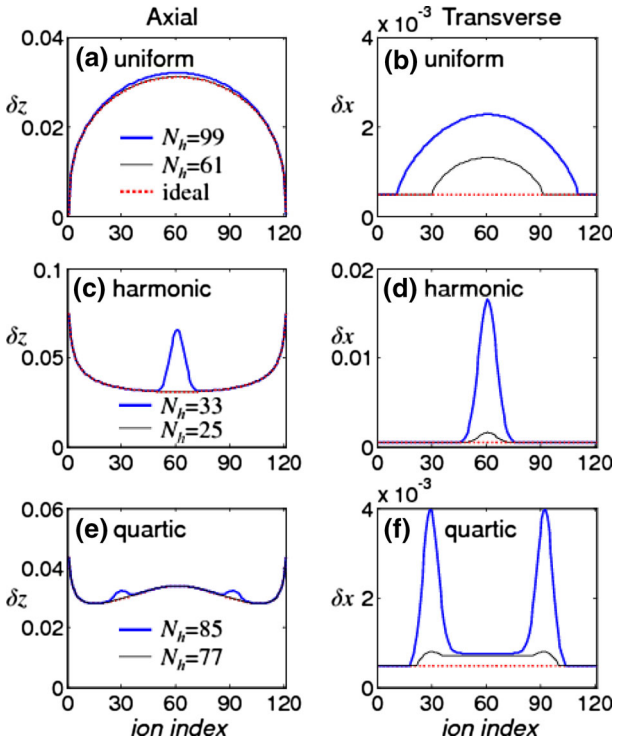

Fig. 3 (Color online) Distributions of the axial and transverse PF (in units of d_0) for various trap geometries under the edge cooling: **a**, **b** a uniform array, **c**, **d** a harmonic trap, **e**, **f** a quartic trap. $(N - N_h)/2$ ions on each end of the ion chain are Doppler cooled with a driven rate $\gamma = 0.1$. For the uniform array, the spacing is $d_0 = 10\mu$m; for the harmonic case, $\omega_z = 2\pi \times 8.4$ kHz and $\omega_x = 2\pi \times 5.1$ MHz, and for the quartic case $\omega_2 \equiv \sqrt{|\alpha_2|/m} = 2\pi \times 5$ kHz and $|\alpha_2/e^2|^{2/3}(\alpha_2/\alpha_4) = -6.2$ such that $\sum_{i=11}^{110}(z_{i+1}^0 - z_i^0)/100 = d_0$. The background heating rate $\kappa = 10^{-4}$ amounts to, for instance, generating 240 phonons per second for the lowest harmonic mode ω_z. Other parameters are the same as used in Fig. 1

a comparison, the corresponding thermal equilibrium profiles at $T = T_D$ are shown as red dotted curves. To consider how many ions can be cooled effectively through sympathetic cooling, we show the curves under different number $N_h \equiv n(H)$ of the computational ions which are subject to the background heating. The axial distribution is shown in Fig. 3a, c, and e. In the uniform case, the curves almost coincide with the ideal thermal equilibrium one under the Doppler temperature, indicating that the system is almost perfectly cooled by sympathetic cooling. In our example with the system size $N = 121$, the edge cooling for a uniform ion chain can afford N_h up to 100 ions, with the maximal δz_i (occurring at the middle ion with $i = 61$) increased by about 4% compared with the ideal case. In the harmonic trap, the affordable N_h is significantly reduced; the ion PF δz_i grows very fast near the chain center as N_h exceeds a certain value ($\sim$25). A considerable improvement can be found in the quartic case, which supports up to $N_h \sim 85$ ions with negligible discrepancy in the distribution. With even larger N_h, humps start to form on two sides instead of being at the chain center. As for the transverse motion, as shown in Fig. 3b, d, and f, the cooling efficiency is in general more vulnerable than that of the axial motion. Because the transverse motion is typically more localized, the ancillary ions have vanishing influences on the ions of increasing distance. It can be observed that although δx_i for the edge ions are fixed by the Doppler temperature, the ions away from the laser-cooled ions soon get large δx_i. Therefore, we expect that it is inefficient to cool the transverse modes with the edge cooling.

The dependence of the cooling efficiency on the number of computational ions N_h is plotted in Fig. 4. To quantify the cooling efficiency, here we look at the maximal axial (transverse) position fluctuation $\delta z^{>}$ ($\delta x^{>}$) among all the ions belonging to H normalized by the middle one's fluctuation δz^0_m (δx^0_m) at the Doppler temperature T_D ($m = 61$ for the system size $N = 121$). With this definition, the normalized characteristic fluctuation approaches the unity when the system reaches the Doppler temperature. With this setup, the sympathetic cooling works better for the axial modes than the transverse ones in terms of the gate infidelities δF^z and δF^x, which are proportional to $\left(\frac{\delta z^{>}}{\delta z^0_{61}}\right)^4$ and $\left(\frac{\delta x^{>}}{\delta x^0_{61}}\right)^4$, respectively. For instance, the infidelity δF^z is roughly increased by 16% for $\frac{\delta z^{>}}{\delta z^0_{61}} \sim 1.04$, but δF^x is increased by 16 times for $\frac{\delta x^{>}}{\delta x^0_{61}} \sim 2$. It is interesting to observe that for both the axial and transverse directions,

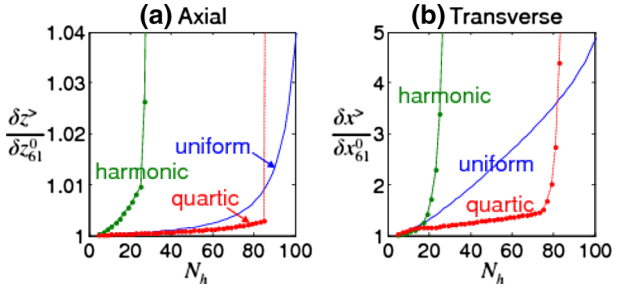

Fig. 4 (Color online) Cooling efficiency (in terms of the normalized PF) as a function of the number of heat-driven ions for **a** the axial and **b** the transverse motion

the curves for the quartic trap rise more slowly than those for the uniform trap before they suddenly jump up around $N_h \sim 85$.

4.2 Periodic-node cooling

As discussed above for the edge cooling, if we impose an efficiency threshold, there must be a limit on N_h beyond which the system cannot be effectively cooled. For long ion chains, therefore, a different spatial arrangement of the cooling ions must be considered. Here, we discuss an improved configuration where the ancillary cooling ions are distributed periodically and evenly in the ion chain. We investigate how the period (the number of computational ions between two adjacent cooling ions/nodes) influences the performance of sympathetic cooling. We still take the ion number $N = 121$ as an example and only Doppler cool the 1st, $(1+P)$th, $(1+2P)$th, ..., Nth ions with a period P that factorizes 120. In Fig. 5, we show the resultant distribution of δx_i and δz_i under three different trapping potentials. Unlike the edge cooling case, a uniform chain has no good performance under the periodic-node cooling. As the reason

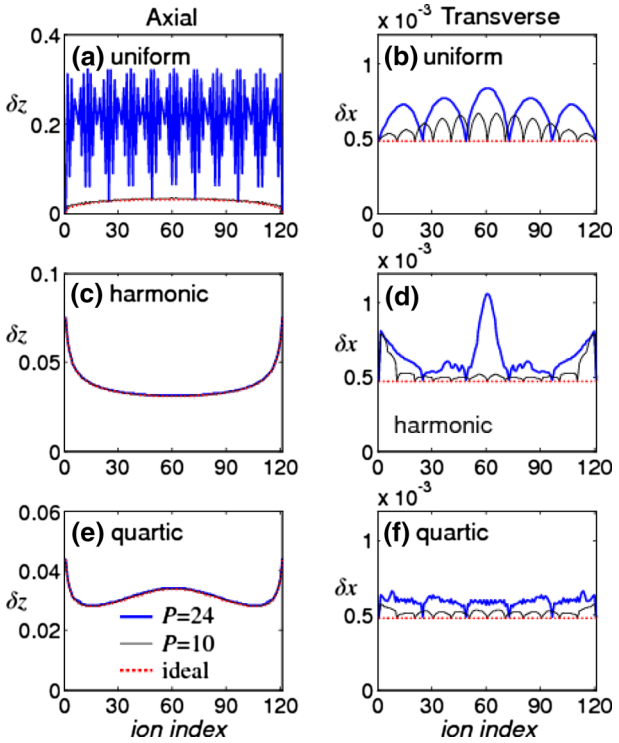

Fig. 5 (Color online) Distributions of the axial and transverse PF (in units of d_0) under the periodic cooling for **a**, **b** a uniform array, **c**, **d** a harmonic trap, **e**, **f** a quartic trap. The total number of ions $N = 121$. All parameters are the same as in Fig. 3 except for the ancilla arrangement. The *curve* legend for all six panels is the same and is given in (**e**)

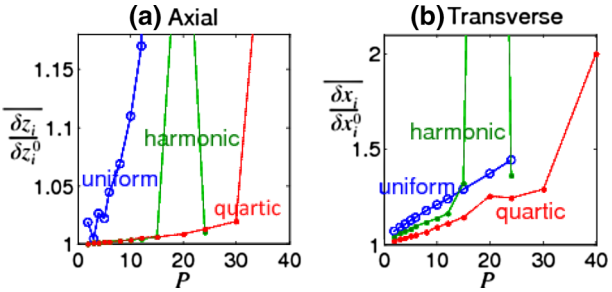

Fig. 6 (Color online) Efficiency of the periodic cooling with different periods of ancilla arrangement for **a** the axial and **b** the transverse motion

will be revealed later in Sect. 5, this is because the cooling rate $\gamma = 0.1$ is not an optimal choice. As for the axial motion in the harmonic and quartic cases shown in Fig. 5c, e, the curves are almost identical to the ideal ones even with a large period $P = 24$ (about 5% of the ions are used for sympathetic cooling in this case). For the transverse direction shown in Fig. 5b, d, and f, δx_i is significantly suppressed compared to those under the edge cooling configuration. Although the detailed distribution depends on the trapping potential, the maximum δx_i is no more than two (1.25) times of δx_i for the ideal case under a large period $P = 24$ ($P = 10$).

We plot the cooling efficiency against the period P in Fig. 6. Here, the efficiency is characterized by $\overline{\frac{\delta z_i}{\delta z_i^0}} \equiv \frac{1}{n(H)} \sum_{i \in H} \frac{\delta z_i}{\delta z_i^0}$ (similarly for $\overline{\frac{\delta x_i}{\delta x_i^0}}$). Note that in the uniform case, the efficiency becomes worse due to the improper choice of $\gamma = 0.1$. For the axial modes shown in Fig. 6a, the efficiency in the harmonic case is as good as that in the quartic case except at $P = 20$, where the ion PF suddenly jumps out of the good range in the harmonic case. For the transverse modes (Fig. 6a), the three trap potentials do not show dramatic differences for $P < 15$, but in general the quartic curve still shows the slowest increase in the ion PF as P gets larger. The exception with a sudden jump of the PF at $P = 20$ is somewhat related to a particular phonon eigenmode structure for the harmonic trap. Such a eigenmode happens to have a few nodal points coincident with the sites of cooling ions. Therefore, this mode cannot be cooled effectively. This can be circumvented by arranging cooling ions asymmetrically with respect to the trap center. On the other hand, if some of the ions happen to be of large PF in one normal mode, cooling these ions effectively cools this mode. So it might be ideal to choose to cool those ions whose amplitudes are large in most of the eigenmodes.

5 Influence of cooling rates

In this section, we discuss the significance of the driving rate γ of the Doppler cooled ions. Intuitively, we would expect that the system can be cooled more efficiently when the driving rate γ gets larger. Our calculation shows that this is however not the case. We study the efficiency with varied γ under the same background heating rate κ. The efficiency characterized by the corresponding (normalized) position fluctuation

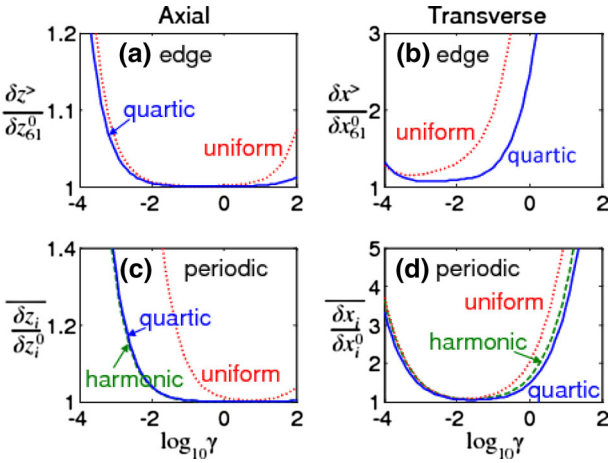

Fig. 7 (Color online) Cooling efficiency for **a** the axial modes and **b** the transverse modes under edge cooling; **c** the axial modes and **d** the transverse modes under periodic-node cooling. The system size $N = 121$. In **a** and **b**, these *curves* correspond to $N_h = 41$. In **c** and **d**, the *curves* correspond to $P = 10$. Other parameters are the same as previously discussed

is plotted in Fig. 7 as a function of γ. Surprisingly, for all the circumstances we consider, the ion position fluctuation first decreases as the driving rate rises in the small γ regime, approaching to a minimum when γ is moderate, and then increases again when γ becomes strong. This suggests that the driving rate has an optimal window for cooling. The fact that the efficiency does not go better with strong cooling rates seems counterintuitive in the first place. But this finding is consistent with our previous work [36]. The reason is that when the driving rate is larger than the inverse of the timescale needed for propagation, the ion is kicked from random directions so frequently that the effects of succeeding kicks cancel out before the first kick is about to "transfer" to its neighbors. If the rate matches the propagation timescale in order of magnitude, the cooling efficiency gets optimal.

Furthermore, these curves do not reach the minima at the same γ; the optimized cooling rate depends on the trapping potentials, cooling configurations, and which direction of the motion is considered. For the edge cooling (Fig. 7a, b), the most efficient window of γ for cooling axial modes lies in the range from 0.1 to 1, both for the uniform and the quartic potentials. With the same rate, the (normalized) transverse PF becomes significantly larger than unity for these two geometries. For the periodic-node cooling (Fig. 7c, d), both the curves for the harmonic and the quartic potentials are nearly identical, with the optimal window lies in the range from $\gamma \sim 0.1$ to 10 for the axial direction and from $\gamma \sim 0.02$ to 0.05 for the transverse direction. By compromising the optimal windows for both the directions, $\gamma \simeq 0.1$ sounds a suitable choice.

6 Relaxation dynamics to the steady state

So far, we have only discussed the steady-state solution to Eq. (2). In this section, we discuss the relaxation timescale toward the steady state, which is also an important

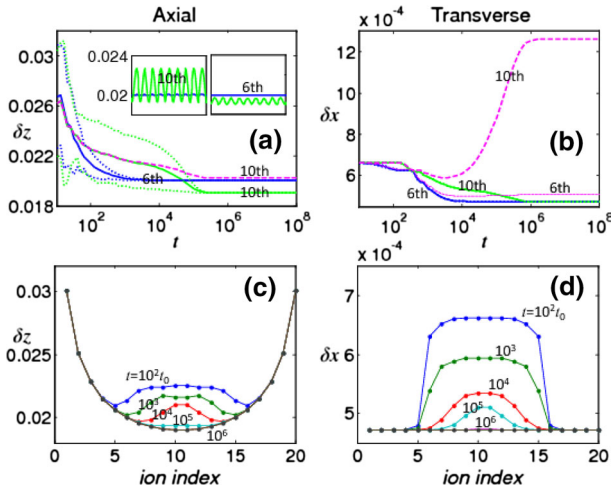

Fig. 8 (Color online) **a**, **b** Temporal profiles of the ion PF for the 6th (*blue curves*) and 10th (*green curves*) ions without considering background heating. In **a**, two *solid lines* represent coarse-grained values since the actual profiles contain fast oscillations as seen in the two insets at $t = 10^4 t_0$ (*left*) and $t = 10^5 t_0$ (*right*), respectively. The coarse-graining interval is $\Delta t/t_0 = 20$. Note that in both insets the time span is $\Delta t'/t_0 = 10$, and the wavy (*green*) behavior belongs to the 10th ion while the PF of the 6th ion stays nearly a constant (*blue*). To show the effect of background heating, the PF profile of the 10th ion is also plotted for comparison (with $\kappa = 10^{-4}$). That of the 6th ion is not explicitly shown because it is almost identical to the *blue solid* (no-heating) curve. In **b**, the fast oscillation amplitude is in the order of $10^{-9} d_0$ so the dotted curves appear to be on top of the solid ones. A thick and a thin (*magenta*) *dotted lines* representing the 10 and 6th ions, respectively, with background heating are also shown for comparison. **c**, **d** The snapshots of the time-averaged distributions and the relevant parameters are the same as Fig. 2

factor concerning the feasibility of employing the sympathetic cooling in experiments. To illustrate the general feature, we first calculate the dynamics of an $N = 20$ ion chain in a harmonic trap under the edge cooling. We assume Doppler cooling is applied to 5 ions on each end of the chain, and the whole chain is initially in thermal equilibrium with temperature $T = 2T_D$. We then plot the curves of δx_i and δz_i with $i = 6$ (right next to the cooling ions) and $i = 10$ (the middle ion) as indicators in Fig. 8a, b. Note that for the axial motion, the two solid lines have been coarse-grained by a small time interval. This is because the actual profiles have very fast oscillations (see the insets of Fig. 8a). We also show the upper and lower envelopes of such oscillations by the dotted lines. The coarse-grained curves asymptotically approach constant values as time increases, along with the fast oscillations dying away gradually. We define a relaxation time τ_R, beyond which the upper envelope falls within 1% of the coarse-grained value. So we find $\tau_R/t_0 \sim 10^5$ for the system to approach the steady state, where $t_0 \equiv 2\pi/\omega_0$ ($\sim 7\mu$s for most of the cases discussed here). For the transverse direction, the amplitude of the fast oscillation is small, but it takes $\tau_R/t_0 \sim 10^6$ to reach the steady state.

Now, we consider the case with background heating at a rate $\kappa = \gamma_{bg} T_{bg} = 10^{-4}$. Different curves corresponding to this case are plotted in dashed lines. Different γ_{bg} changes the final distribution of δx_i and δz_i, but do not lead to significant variation in the relaxation timescale. Figure 8c, d shows the snapshots of the distribution of

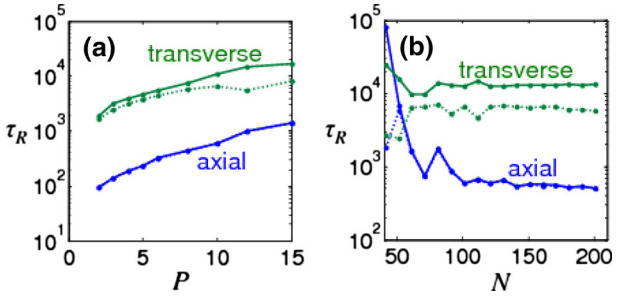

Fig. 9 (Color online) Relaxation time τ_R as a function of **a** the period P in the periodic-node cooling for $N = 121$, and **b** the total length N of the ion chain for a given $P = 10$. The *solid curves* correspond to no background heating cases, and the *dotted lines* correspond to background heating cases with $\kappa = 10^{-4}$. For **a** the relevant parameters are the same as Fig. 5. For chains of different sizes in **b** the quartic trap is determined by minimizing $\sum_{i=16}^{N-16}(z_{i+1}^0 - z_i^0)^2/(N-31)$ and setting $\sum_{i=16}^{N-16}(z_{i+1}^0 - z_i^0)/(N-31) = d_0$

δx_i and δz_i (coarse-graining also applied to the axial mode) at different times. The cooling ions immediately reach their steady states (in a short timescale γ^{-1} which is not visible from the curve). The cooling then starts to propagate to the inner part of the ion chain.

Previous discussion has shown that the relaxation time of edge cooling is still quite long (0.1 to 1 second). We then turn to the more efficient periodic-node cooling for a large ion chain. We here consider a quartic trap and examine the relaxation time τ_R as a function of the period P. As expected, Fig. 9a shows that τ_R is in general an increasing function with P. For an $N = 121$ chain, we find the timescale can be controlled within $\tau_R/t_0 \sim 10^4$ (tens of milliseconds) while the axial relaxation takes roughly 10 times shorter than the transverse one. These results show a timescale comparable to usual Doppler cooling (of order of a few milliseconds). If the background heating is included, the transverse curve drops slightly, but the axial curve is hardly affected. As more ions are added into the system, it is important to make sure that the relaxation time does not scale up too fast with N. We show in Fig. 9b the scaling curves of τ_R with increasing N by fixing $P = 10$. The axial relaxation time tends to decrease as the system size increases and meets a lower bound in the large N limit. On the contrary, the transverse relaxation time appears to be independent of N. This is because the transverse motion tends to involve only nearby ions. So a longer chain is nothing but a simple repetition of segments of a size P.

7 Conclusion

To conclude, we have presented a detailed investigation on the sympathetic cooling in a large ion chain. Many findings discovered in this paper are instructional for experimental implementation. First, a steady state can be reached for a system subject to constant background heating under continuous sympathetic cooling. By arranging cooling ancillary ions in different ways, the cooling performance can be improved and optimized. In our calculation, although the transverse motion is relatively harder to be cooled than the axial one, by inserting ancillary ions evenly over the chain, it can

be cooled down to a satisfactory level. We have studied the effect of cooling rates and found the optimal window of the cooling rates. We have also discussed the relaxation dynamics and showed that the required timescale is within the reach of experiments.

Acknowledgments This work was supported by the NBRPC 2011CBA00302, the IARPA MUSIQC program, the AFOSR and the ARO MURI program, and the support from National Taiwan University under Grants No. NTU-ERP-103R891401, NTU-ERP-103R891402, and NTU-ERP-103R104021.

References

1. Sørensen, A., Mølmer, K.: Quantum computation with ions in thermal motion. Phys. Rev. Lett. **82**(9), 1971–1974 (1999)
2. Milburn, G.J., Schneider, S., James, D.F.V.: Ion trap quantum computing with warm ions. Fortschr. Phys. **48**(9–11), 801–810 (2000)
3. Sørensen, A., Mølmer, K.: Entanglement and quantum computation with ions in thermal motion. Phys. Rev. A **62**(2), 022311 (2000)
4. Leibfried, D., DeMarco, B., Meyer, V., Lucas, D., Barrett, M., Britton, J., Itano, W.M., Jelenković, B., Langer, C., Rosenband, T., Wineland, D.J.: Experimental demonstration of a robust, high-fidelity geometric two ion-qubit phase gate. Nature **422**(6930), 412–415 (2003)
5. Myerson, A.H., Szwer, D.J., Webster, S.C., Allcock, D.T.C., Curtis, M.J., Imreh, G., Sherman, J.A., Stacey, D.N., Steane, A.M., Lucas, D.M.: High-fidelity readout of trapped-ion qubits. Phys. Rev. Lett. **100**(20), 200502 (2008)
6. Burrell, A.H., Szwer, D.J., Webster, S.C., Lucas, D.M.: Scalable simultaneous multiqubit readout with 99.99% single-shot fidelity. Phys. Rev. A **81**(4), 040302 (2010)
7. Harty, T.P., Allcock, D.T.C., Ballance, C.J., Guidoni, L., Janacek, H.A., Linke, N.M., Stacey, D.N., Lucas, D.M.: High-fidelity preparation, gates, memory, and readout of a trapped-ion quantum bit. Phys. Rev. Lett. **113**(22), 220501 (2014)
8. Sackett, C.A., Kielpinski, D., King, B.E., Langer, C., Meyer, V., Myatt, C.J., Rowe, M., Turchette, Q.A., Itano, W.M., Wineland, D.J., Monroe, C.: Experimental entanglement of four particles. Nature **404**(6775), 256–259 (2000)
9. Leibfried, D., Knill, E., Seidelin, S., Britton, J., Blakestad, R.B., Chiaverini, J., Hume, D.B., Itano, W.M., Jost, J.D., Langer, C., Ozeri, R., Reichle, R., Wineland, D.J.: Creation of a six-atom 'Schrödinger cat' state. Nature **438**(7068), 639–642 (2005)
10. Häffner, H., Hänsel, W., Roos, C.F., Benhelm, J., Chek-al-kar, D., Chwalla, M., Körber, T., Rapol, U.D., Riebe, M., Schmidt, P.O., Becher, C., Gühne, O., Dür, W., Blatt, R.: Scalable multiparticle entanglement of trapped ions. Nature **438**(7068), 643–646 (2005)
11. Monz, T., Schindler, P., Barreiro, J.T., Chwalla, M., Nigg, D., Coish, W.A., Harlander, M., Hänsel, W., Hennrich, M., Blatt, R.: 14-qubit entanglement: creation and coherence. Phys. Rev. Lett. **106**(13), 130506 (2011)
12. Noguchi, A., Toyoda, K., Urabe, S.: Generation of Dicke states with phonon-mediated multilevel stimulated Raman adiabatic passage. Phys. Rev. Lett. **109**, 260502 (2012)
13. Jurcevic, P., Lanyon, B.P., Hauke, P., Hempel, C., Zoller, P., Blatt, R., Roos, C.F.: Quasiparticle engineering and entanglement propagation in a quantum many-body system. Nature **511**(7508), 202–205 (2014)
14. Lanyon, B.P., Zwerger, M., Jurcevic, P., Hempel, C., Dür, W., Briegel, H.J., Blatt, R., Roos, C.F.: Experimental violation of multipartite bell inequalities with trapped ions. Phys. Rev. Lett. **112**, 100403 (2014)
15. Northup, T.: Quantum physics: squeezed ions in two places at once. Nature **521**(7552), 295–296 (2015)
16. Riebe, M., Häffner, H., Roos, C.F., Hänsel, W., Benhelm, J., Lancaster, G.P.T., Körber, T.W., Becher, C., Schmidt-Kaler, F., James, D.F.V., Blatt, R.: Deterministic quantum teleportation with atoms. Nature **429**(6993), 734–737 (2004)
17. Olmschenk, S., Matsukevich, D.N., Maunz, P., Hayes, D., Duan, L.-M., Monroe, C.: Quantum teleportation between distant matter qubits. Science **323**(5913), 486–489 (2009)
18. Kielpinski, D., Monroe, C., Wineland, D.J.: Architecture for a large-scale ion-trap quantum computer. Nature **417**(6890), 709–711 (2002)

19. Bowler, R., Gaebler, J., Lin, Y., Tan, T.R., Hanneke, D., Jost, J.D., Home, J.P., Leibfried, D., Wineland, D.J.: Coherent diabatic ion transport and separation in a multizone trap array. Phys. Rev. Lett. **109**, 080502 (2012)
20. Walther, A., Ziesel, F., Ruster, T., Dawkins, S.T., Ott, K., Hettrich, M., Singer, K., Schmidt-Kaler, F., Poschinger, U.: Controlling fast transport of cold trapped ions. Phys. Rev. Lett. **109**, 080501 (2012)
21. Duan, L.-M., Madsen, M.J., Moehring, D.L., Maunz, P., Kohn, R.N., Monroe, C.: Probabilistic quantum gates between remote atoms through interference of optical frequency qubits. Phys. Rev. A **73**(6), 062324 (2006)
22. Moehring, D.L., Maunz, P., Olmschenk, S., Younge, K.C., Matsukevich, D.N., Duan, L.-M., Monroe, C.: Entanglement of single-atom quantum bits at a distance. Nature **449**(7158), 68–71 (2007)
23. Duan, L.-M., Monroe, C.: Quantum networks with trapped ions. Rev. Mod. Phys. **82**(2), 1209–1224 (2010)
24. Northup, T.E., Blatt, R.: Quantum information transfer using photons. Nat Photon **8**(5), 356–363 (2014)
25. Monroe, C., Raussendorf, R., Ruthven, A., Brown, K.R., Maunz, P., Duan, L.-M., Kim, J.: Large-scale modular quantum-computer architecture with atomic memory and photonic interconnects. Phys. Rev. A **89**, 022317 (2014)
26. Hucul, D., Inlek, I.V., Vittorini, G., Crocker, C., Debnath, S., Clark, S.M., Monroe, C.: Modular entanglement of atomic qubits using photons and phonons. Nat Phys **11**(1), 37–42 (2015)
27. Wineland, D.J., Monroe, C., Itano, W.M., Leibfried, D., King, B.E., Meekhof, D.M.: Experimental issues in coherent quantum-state manipulation of trapped atomic ions. J. Res. Natl. Inst. Stand. Tech. **103**, 259 (1998)
28. Leibfried, D., Blatt, R., Monroe, C., Wineland, D.: Quantum dynamics of single trapped ions. Rev. Mod. Phys. **75**(1), 281–324 (2003)
29. Lin, G.-D., Zhu, S.-L., Islam, R., Kim, K., Chang, M.-S., Korenblit, S., Monroe, C., Duan, L.-M.: Large-scale quantum computation in an anharmonic linear ion trap. Europhys. Lett. **86**(6), 60004 (5pp) (2009)
30. Zhu, S.-L., Monroe, C., Duan, L.M.: Trapped ion quantum computation with transverse phonon modes. Phys. Rev. Lett. **97**(5), 050505 (2006)
31. Larson, D.J., Bergquist, J.C., Bollinger, J.J., Itano, W.M., Wineland, D.J.: Sympathetic cooling of trapped ions: a laser-cooled two-species nonneutral ion plasma. Phys. Rev. Lett. **57**(1), 70–73 (1986)
32. Kielpinski, D., King, B.E., Myatt, C.J., Sackett, C.A., Turchette, Q.A., Itano, W.M., Monroe, C., Wineland, D.J., Zurek, W.H.: Sympathetic cooling of trapped ions for quantum logic. Phys. Rev. A **61**(3), 032310 (2000)
33. Barrett, M.D., DeMarco, B., Schaetz, T., Meyer, V., Leibfried, D., Britton, J., Chiaverini, J., Itano, W.M., Jelenković, B., Jost, J.D., Langer, C., Rosenband, T., Wineland, D.J.: Sympathetic cooling of $^{9}Be^{+}$ and $^{24}Mg^{+}$ for quantum logic. Phys. Rev. A **68**(4), 042302 (2003)
34. Home, J.P., McDonnell, M.J., Szwer, D.J., Keitch, B.C., Lucas, D.M., Stacey, D.N., Steane, A.M.: Memory coherence of a sympathetically cooled trapped-ion qubit. Phys. Rev. A **79**(5), 050305 (2009)
35. Brown, K.R., Ospelkaus, C., Colombe, Y., Wilson, A.C., Leibfried, D., Wineland, D.J.: Coupled quantized mechanical oscillators. Nature **471**(7337), 196–199 (2011)
36. Lin, G.-D., Duan, L.-M.: Equilibration and temperature distribution in a driven ion chain. New J. Phys. **13**, 075015 (2011)